

Homogeneous bubble nucleation in water at negative pressure: A Voronoi polyhedra analysis

Jose L. F. Abascal, Miguel A. Gonzalez, Juan L. Aragoes and C. Valeriani

*Departamento de Química Física, Facultad de Ciencias Químicas,
Universidad Complutense de Madrid, 28040 Madrid, Spain*

(Dated: February 23, 2022)

Abstract

We investigate vapor bubble nucleation in metastable TIP4P/2005 water at negative pressure via the Mean First Passage Time (MFPT) method using the volume of the largest bubble as a local order parameter. We identify the bubbles in the system by means of a Voronoi-based analysis of the Molecular Dynamics trajectories. By comparing the features of the tessellation of liquid water at ambient conditions to those of the same system with an empty cavity we are able to discriminate vapor (or interfacial) molecules from the bulk ones. This information is used to follow the time evolution of the largest bubble until the system cavitates at 280 K above and below the spinodal line. At the pressure above the spinodal line, the MFPT curve shows the expected shape for a moderately metastable liquid from which we estimate the bubble nucleation rate and the size of the critical cluster. The nucleation rate estimated using Classical Nucleation Theory turns out to be about 8 order of magnitude lower than the one we compute by means of MFPT. The behavior at the pressure below the spinodal line, where the liquid is thermodynamically unstable, is remarkably different, the MFPT curve being a monotonous function without any inflection point.

I. INTRODUCTION

Bubble nucleation is a widespread phenomenon in our daily life, relevant to processes such as explosive boiling¹ and sonochemistry². Despite its technological relevance, the mechanism of nucleation of vapor bubbles from homogeneous metastable liquids is still not entirely understood. Classical Nucleation Theory (CNT) is usually employed to predict the nucleation rate, both in bubble nucleation and in vapor condensation experiments. Early measurements of vapor condensation estimated nucleation rates consistent with the CNT predictions.³ Regarding bubble nucleation, measurements on different materials^{4–11} have shown that, even though Classical Nucleation Theory correctly predicts the temperature dependence of the bubble nucleation rate, it yields nucleation rates that are too low at the lowest temperatures. Delale et al.,¹² using a phenomenological estimate of the minimum work of bubble formation, computed the steady-state bubble nucleation rate and found that, as with the CNT estimates, there was a large discrepancy between the computed and measured bubble-nucleation rates. Recently, El Mekki Azouzi et al.¹³, performing experiments of liquid water under large mechanical tension, used the cavitation statistics to get the free-energy barrier. The authors observed that both the free energy and the volume of the critical bubble were well described by CNT whereas the surface tension was reduced.

From a theoretical and numerical point of view, Zeng and Oxtoby¹⁴ used Density Functional Theory to estimate the bubble nucleation rate in a super-heated Lennard Jones system and concluded that CNT underestimated the nucleation rate by more than 15 orders of magnitude. One reason for it was that CNT neglects curvature corrections to the surface free-energy of the bubble¹⁵. In 1999, Shen and Debenedetti¹⁶ performed a computer simulation study of bubble nucleation from a metastable super-heated Lennard Jones system. Using the vapor density as a global order parameter, they found that the critical nucleus was a large system-spanning cavity, in contrast to the spherical cluster predicted with CNT. Later on, Wang et al.¹⁷ reported a Molecular Dynamic study of homogeneous bubble nucleation for the same Lennard-Jones fluid. Using Forward Flux Sampling and the volume of the largest bubble as a local order parameter, they computed the bubble nucleation rate at a given super-heating and obtained $10^{-22}\sigma^{-3}\tau^{-1}$. At the same conditions, the CNT estimate could vary from $10^{-22}\sigma^{-3}\tau^{-1}$ to $10^{-36}\sigma^{-3}\tau^{-1}$, depending on the value of the interfacial tension (whether obtained from MD or DFT calculations) used to estimate the

free-energy barrier height. The authors also observed that local temperature fluctuations correlated strongly with bubble formation (mechanism not taken into account in CNT) and that, contrary to Ref. 16, cavitation started from compact bubbles. Recently, Meadley and Escobedo¹⁸ studied the same Lennard Jones metastable fluid, undergoing not only superheating but also over-stretching (negative pressure). The authors used several rare-event numerical techniques and both a local (the volume of the largest bubble) and a global order parameter (the global vapor density) to follow the liquid to vapor phase transition and estimated the nucleation rate and the free-energy barrier. They found that the free-energy barrier was higher when projected over the bubble volume rather than over the vapor density and concluded that the former was a more ideal reaction coordinate. When analyzing the shape of the growing vapor bubble, they observed bubbles with non-spherical shapes and irregular and undulating surfaces.

In contrast to the work done to unravel the bubble nucleation mechanism in simple fluids (such as Lennard Jones), little effort has been made so far to understand the mechanism behind the liquid to vapor transition in molecular liquids such as water. The goal of the present manuscript is to study bubble nucleation in numerical simulations of TIP4P/2005 water at negative pressures using the size of the largest bubble as a local order parameter. The bubble volume is obtained by means of a Voronoi-based algorithm. Knowing the location of the spinodal line for TIP4P/2005 water at negative pressures,¹⁹ we study bubble nucleation for two state points located, respectively, slightly above and below the spinodal. In both cases the system cavitated spontaneously. Therefore, the *Mean First Passage Time* (MFPT) method^{20,21} seemed to be adequate to compute the bubble nucleation rate and to estimate the volume of the critical bubble. MFPT has been successfully applied to study liquid condensation from metastable vapor in a Lennard-Jones system^{22,23} and from metastable TIP4P/2005 water²⁴. The application of the MFPT technique to bubble nucleation ultimately relies in the investigation of the time evolution of the bubble growth. The detection of bubbles in computer generated configurations of a metastable liquid is more complex than it may appear at first. A number of procedures have been proposed to distinguish liquid-like from vapor-like particles.^{25–27} A bubble is a region of vapor within the liquid and since the vapor is much less dense than the liquid (except in the vicinity of the critical point), in principle, one might think of a bubble as a “void” region. Given the small size of the bubble, it is difficult to know to what extent the interface affects the

structure of the vapor molecules. The problem is more complex for a network forming liquid such as water whose structure is not determined exclusively by packing effects since the hydrogen bond network is a structure with many voids. Because of this, the fixed cutoff criterion of Ref.28 which has been successfully employed in the analysis of the condensation of a metastable Lennard-Jones vapor might not work in the case of water. We thus face a challenging geometrical problem.

The procedure to tag the molecules as either liquid or vapor may be performed in three steps: 1) A partition of the space between the molecules into regions, 2) An assignment of each region as belonging to a "vapor" (or interfacial) or a liquid molecule, and 3) A clustering of the vapor molecules into bubbles. To solve the first step, the Voronoi (also known as Dirichlet) tessellation is a natural choice leading to an unambiguous partition of the system. The Voronoi construction is a partition of the space based on the distance to a set of points. Each region contains exactly one generating point and every point in a given region is closer to its generating point than to any other. The Voronoi tessellation has been found useful in many scientific and technical applications.²⁹⁻³² When the space is Euclidean and the set of points are physical or chemical particles, it allows to univocally assign a given region to every particle—a polygon in 2D and a polyhedron in 3D—thus providing structural information of the system. To our knowledge, the first application of the tessellation to elucidate the structure of a chemical-physics system was done by Bernal in 1964.³³ Since then a number of studies have used the Voronoi tessellation to investigate the structure of fluids, glasses and solids.³⁴⁻⁴⁵ Other typical examples of the utility of the Voronoi construction are the analysis of solvation shells,⁴⁶⁻⁴⁹ clustering and chemical association.^{36,50-52} The Voronoi construction has also been employed to define the interface between two systems⁵³⁻⁵⁵ and to obtain structural information of pure water.^{50,56-62} and water solutions^{36,63-69} More closely related with the goals of this work is its application to detect different types of cavities such as pores, pockets, clefts, channels and docking sites.^{50,70-79} In fact, Fern *et al.*⁸⁰ have already used the Voronoi tessellation as a tool for distinguishing whether a particle belongs to a condensed or vapor phase in two-phase simulations of ethanol.

The Voronoi tessellation can be performed trivially in crystalline systems but it becomes increasingly complex in disordered systems.^{35,36,77,81,82} In fact, when the system is strongly heterogeneous (as is the case of bubbles within a metastable liquid) many algorithms fail. In this work we use an algorithm especially designed to deal with inhomogeneous fluids which

has been successfully applied to interpret the structure of quenched liquids³⁵ and electrolyte solutions.³⁶ Once the tessellation is done, the properties of the Voronoi polyhedra (VP) associated to each particle can be used to distinguish between liquid and vapor molecules. The choice of the parameters that denote a molecule as belonging to the vapor phase is somewhat arbitrary. Therefore, as a test case, we have investigated the properties of a system consisting of liquid water with an artificially created spherical cavity. Once the vapor molecules are identified with the Voronoi construction, it is a trivial task to cluster them into one or more bubbles because the Voronoi tessellation directly provides the list of neighbors of each molecule. We then use the volume of the largest bubble as the order parameter and apply the MFPT technique to study the spontaneous bubble nucleation.²⁰ The analysis of the evolution of the volume of the largest bubble provides the desired relevant features of the nucleation, in particular the nucleation rate and the size (volume) of the critical bubble. In this work we will show that the overall procedure is quite robust and yields a consistent description of the bubble nucleation.

The main drawback of the overall method is that the Voronoi tessellation is far from trivial for highly inhomogeneous systems. We have thus dedicated a section to describe the algorithm used for the tessellation and another one to investigate what are the relevant parameters of the tessellation that enable us to track down the bubble growth. The paper is organized as follows. Section II describes some methodological issues, in particular, the algorithm employed for the Voronoi construction and a brief description of the simulations. Section III analyzes which are the relevant parameters of the Voronoi Polyhedra that allow to detect a bubble within metastable liquid water. Finally, section IV reports the application of the MFPT technique to two state points, one above and the other below the liquid- vapor spinodal line of TIP4P/2005 water.

II. METHODS

A. Algorithm used for the Voronoi tessellation

The Voronoi tessellation involves the calculation of the intersection of the planes normal to the line joining a given particle with the remaining ones. Usually, in simple liquids, the number of Voronoi neighbors is less than twenty. It is then a waste of resources evaluating

the normal planes for all particles in the system. Thus, it is customary to perform the calculations for a reduced set of particles, the so called "candidate neighbors".

The list of candidate neighbors of each particle is usually obtained using a cutoff radius. This procedure works well for common liquids but fails for inhomogeneous systems^{35,36} because some actual Voronoi neighbors are relatively distant from the reference particle. In the case of a bubble some Voronoi neighbors may be found at distances of the order of the bubble diameter so the number of candidate neighbors may well exceed a hundred particles. Thus, it is important to devise a different way to obtain a reliable list of candidate neighbors without the computational cost associated to a very large cutoff. As in Ref. 35, the procedure we follow can be described in few steps.

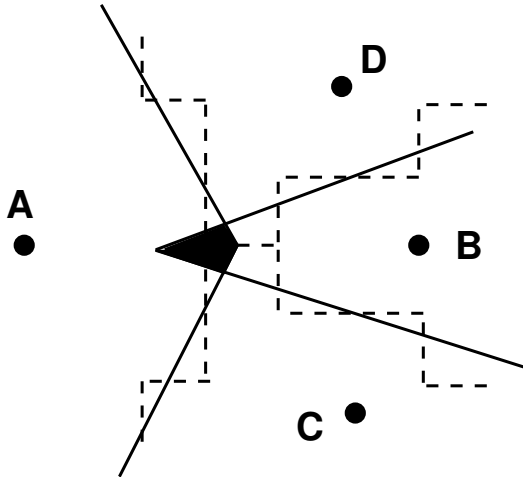
Step1: First, we obtain a first approximation of each particle's list of Voronoi candidate neighbors. This is done by dividing the system in boxes with the use of a grid, each box being assigned to its closest particle. Therefore, two particles are nearest candidate neighbors if at least two boxes (each box belonging to a particle) are adjacent. Rigorously, this stage of the algorithm only works in the limit of zero thickness grid. Thus, we need to improve this initial list of candidates.

Step 2: To amend the calculated set of candidate neighbors, the atoms sharing a certain number of common neighbors with a given one are recursively added to its list of candidates (see Fig. 1). At the end of this stage, we have generated a set of candidates for each particle that hopefully includes all the actual Voronoi neighbors.

Step 3: Having the list of candidate neighbors for all the particles, we proceed with the tessellation using any standard algorithm.⁸³⁻⁸⁶ For this final third step we choose to use a variation of the Finney's algorithm⁸⁴ in order to increase its efficiency (see Ref. 35 for details and a forthcoming paper⁸⁷).

The main advantage of the algorithm is its robustness. However, the large inhomogeneities of our systems have forced us to use it choosing parameters in a conservative way. We have used a 200x200x200 grid and performed the neighbor expansion with a reduced number (6) of common neighbors. In these conditions, the number of actual Voronoi neighbors can be sometimes close to 40. With these parameters, we have been able to analyze all the generated configurations (about $8 \cdot 10^5$ in total) before the system cavitates.

FIG. 1: Particles A and B have not been identified by the grid as Voronoi neighbours. As a consequence the filled region would be ascribed to both particles (and it would be counted twice). Since A and B have C and D as common neighbors, the expansion of the initial list for A and B to include particles with a given number of common neighbors (see step 2 in the text) would allow to divide the filled volume among A and B.



We have carried out 200 independent Molecular Dynamics simulation runs for each of the state points of liquid water at 280 K. One of them, at $p=-2250$ bar, is above the spinodal line and the other one, at $p=-2630$ bar, is below it (recently, a first approach to the spinodal line at low temperatures has been reported for this model¹⁹). All simulations have been performed for 500 water molecules in the isothermal-isobaric NpT ensemble using the Molecular Dynamics package GROMACS⁸⁸ with a 1 fs timestep. Long range electrostatic interactions have been evaluated with the smooth Particle Mesh Ewald method.⁸⁹ The geometry of the water molecules has been enforced using *ad hoc* constraints.⁹⁰ Temperature has been set to the desired value with a velocity rescaling thermostat⁹¹ and, to keep the pressure constant, an isotropic Parrinello-Rahman barostat has been applied.⁹² We have used the TIP4P/2005 model⁹³ to describe the interactions between water molecules. This model provides a quantitative account of many water properties,^{94,95} including not only the well known thermodynamic anomalies,⁹⁶ but also the dynamical ones.⁹⁷ Of particular relevance for the purposes of this work is the high quality of the predictions for the vapor-liquid equilibria.⁹⁸ It is finally to be mentioned that the TIP4P/2005 model has been successfully used to study the nucleation of liquid droplets within a metastable vapor.²⁴

III. VORONOI TESSELLATION AS A TOOL FOR DETECTING BUBBLES

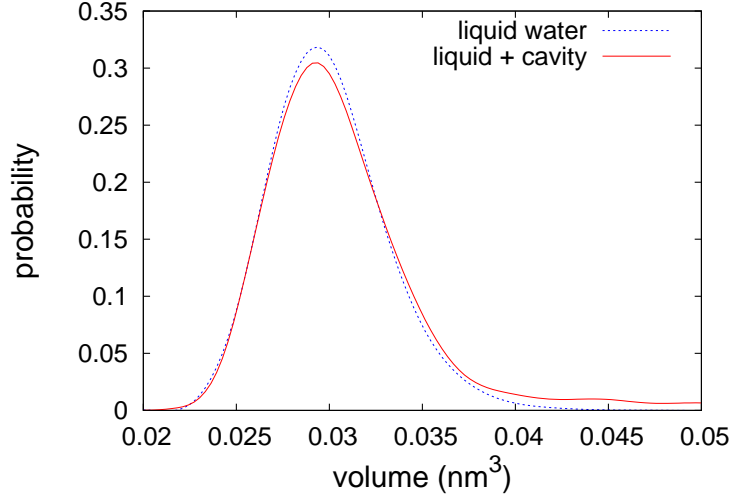
A. Test case: Liquid water with an empty cavity

Our goal is to detect the formation and growth of one or more bubbles within metastable liquid water. Therefore, we need a criterion to distinguish between vapor and liquid particles. Given the density difference between vapor and liquid, a bubble will contain few vapor molecules surrounded by liquid ones. Thus, to a first approximation, a bubble appears as a “void” in the liquid. It is then probably simpler to detect the bubble using the location of the interfacial molecules. To better characterize the interfacial molecules, we analyse the differences between the Voronoi Polyhedra (VP) obtained for a given number of configurations of bulk water at 298 K and 1 bar and the VP computed for the same configurations where we have artificially created an empty spherical cavity by removing 30 water molecules (this approximately corresponds to a 0.6 nm cavity radius and a 0.90-0.95 nm³ volume). Using the Voronoi tessellation, we compute properties such as the VP volume and the non-sphericity parameter (i.e., a measure of the deviation of the Voronoi Polyhedra from a spherical shape). The differences between these properties have to be attributed to the interfacial molecules around the cavity since the remaining particles have exactly the same environment. We may then find what are the VP properties that allow to discriminate interfacial particles (only present in the system with a cavity) from the bulk ones (common to both systems). We note that the Voronoi tessellations have been done using only the positions of the oxygen atoms.

Figure 2 compares the normalized distribution of the VP volumes for a 500 molecules system (470 in the system with the cavity). Clearly, the volume distributions are identical (taken into account the different number of particles in each system) up to a VP volume of about 0.032 nm³. Larger volumes in the system with the cavity outnumber the corresponding ones in the bulk due to the fact that the tessellation assigns the empty space to the “interfacial” particles. This increase is progressive but, for volumes between 0.032 nm³ and 0.04 nm³, it is difficult to label the molecules as either bulk or interfacial based only on this criterion since these volumes appear in more or less similar proportions in both systems. Molecules with VP volumes larger than 0.04 nm³ are almost inexistent in the bulk system while they represent a small but significant part of the total molecules in the system with a

cavity.

FIG. 2: Distribution of VP volumes for TIP4P/2005 water at 298 K, 1 bar. The difference between the systems is that in one of them an empty spherical cavity of 30 molecules has been created.



In order to better distinguish bulk from interfacial molecules, it seems necessary to use another parameter obtained from the VP tessellation. The non-sphericity (or asphericity) parameter has been widely used for that purpose.^{32,50,57,60,62,99–101} Sometimes the definition of the Voronoi Polyhedra anisotropy is made in terms of the VP surface and volume but a more rigorous definition should also involve the mean curvature radius. Thus, we define the nonsphericity parameter, or anisotropic factor α , with the usual expression valid for convex bodies, namely

$$\alpha = RS/3V \quad (1)$$

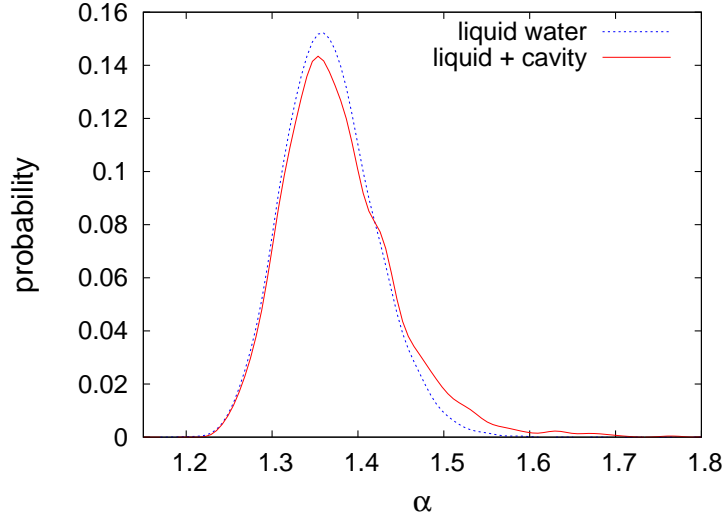
where S and V are the surface and volume of the convex body, respectively, and R the mean curvature radius. In some cases, the geometry of the convex body makes difficult the evaluation of R . This is not the case of a convex polyhedron for which a simple expression allows the calculation of R :

$$R = \frac{1}{8\pi} \sum l_i \phi_i, \quad (2)$$

where the sum extends over polyhedron edges of length l_i and ϕ_i is the angle between the normal vectors to the intersecting faces. These magnitudes are trivially evaluated in

the VP tessellation, so a rigorous calculation of α is numerically possible. As a reference, the nonsphericity parameter of a sphere is 1 and the distribution of α for a representative Lennard-Jones liquid has a maximum at about 1.3.³⁵

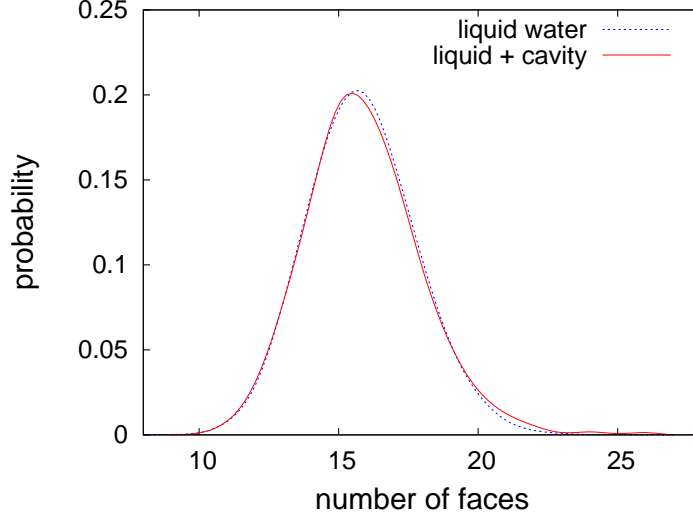
FIG. 3: Distribution of VP nonsphericity factors for the systems of Fig. 1



The nonsphericity factors of the VP for the liquid and the liquid with a cavity systems are shown in Figure 3. The larger anisotropy of the interfacial molecules around the cavity gives rise to a hump in the distribution function. But, similarly to the case of the volume distribution, there is a range of anisotropies (approximately $1.4 < \alpha < 1.5$) which may correspond to either bulk or interfacial molecules making difficult to distinguish between them. Only when $\alpha > 1.5$ one may be reasonably confident that the nonsphericity parameter represents interfacial molecules.

Therefore, both the VP volume and anisotropy allow to unambiguously characterize only a part of the interfacial molecules, *i.e.*, those with $V > 0.40 \text{ nm}^3$ or $\alpha > 1.5$. Thus, we need additional parameters in order to improve the particles' assignment (whether liquid or vapor-like). The VP number of faces has been sometimes proposed as a relevant structural parameter. However this seems not to be the case for water. Figure 4 shows that the distribution of faces is quite similar in both systems and does not provide any additional information. It is worth comment that, in liquid water, a non-negligible number of Voronoi Polyhedra has more than 20 faces and this number is over 30 for some interfacial molecules, which explains the difficulties in designing a robust algorithm for the Voronoi tessellation.

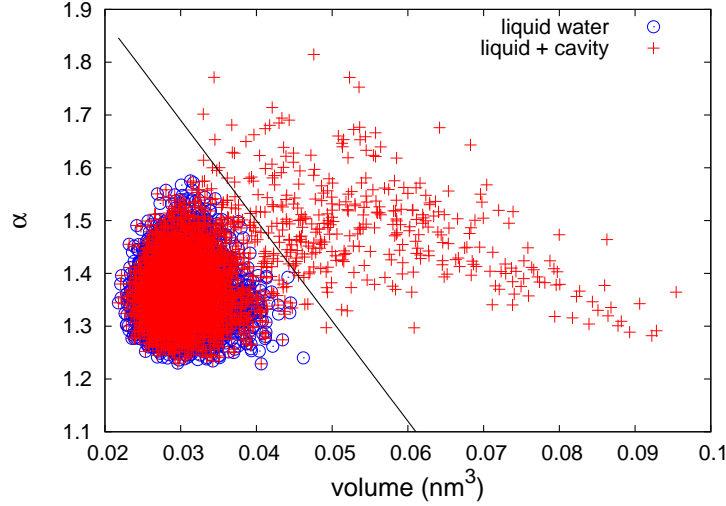
FIG. 4: Distribution of VP number of faces for the systems of Fig. 1



Since the use of a single parameter, either V or α , does not allow an unequivocal assignment of the interfacial molecules, we suggest to use a correlation of both parameters in order to enhance the ability to detect them. Figure 5 represents the values of α for 11 randomly selected configurations plotted against their corresponding volumes. Notice that the points for the liquid system (without cavity) are grouped in a relatively small “pear-shaped” region of the α - V plane. Most of these points overlap with those of the system with a cavity because they correspond to the common (bulk) molecules. On the right side of the figure appear only points coming from the system with a cavity. These must be ascribed to the molecules surrounding the cavity (interfacial molecules) because their environments are different in both systems.

Therefore, the parameters useful to identify the interfacial molecules are clearly visible in this plot. In the figure we have also traced a straight line ($\alpha = 1.5 - 19 \cdot (V - 0.04)$) separating two regions: all the liquid-like (bulk) particles lie to the left of the line while most of the points specific of the system with a cavity (interfacial molecules) are on the right side of the line. One could argue that the position of the line could be shifted slightly to the left but we opted for a conservative approach. In fact, the line pivots around the point ($v = 0.04 \text{ nm}^3$, $\alpha = 1.5$) which was previously shown to clearly indicate that a particle is interfacial. We

FIG. 5: Anisotropic factor α as a function of volume for the systems of Fig. 1. The black line $\alpha = 1.5 - 19 * (V - 0.04)$ separates bulk molecules from interfacial molecules.



also stress that the sample used for the figure is relatively small (only 11 configurations out of about 500 molecules for each system). Plotting a larger number of configurations would imply the appearance of a larger number of molecules with parameters in the right side of the distribution tails (with large values of both volumes and anisotropies), and some among them in the interfacial region. In summary, we recommend a linear combination of the VP volume and anisotropy α to ensure that no bulk particles are tagged as interfacial even if it slightly underestimates the number of the latter. As shown, the use of this parameter is highly discriminating and allows to safely detect most of the interfacial molecules.

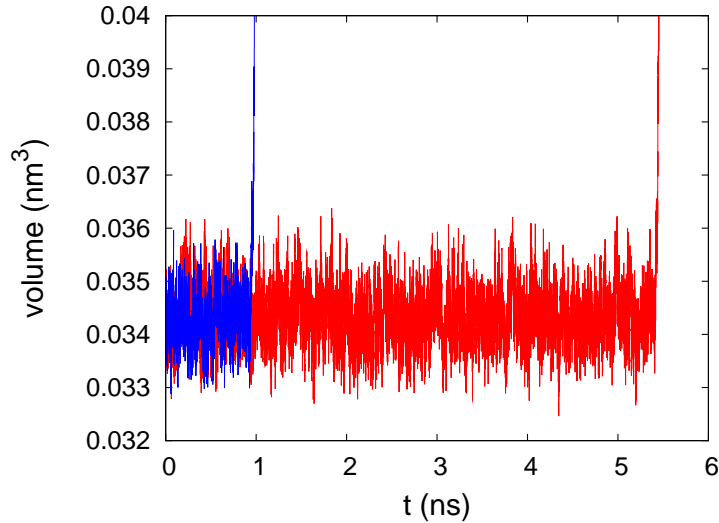
The advantage of the analysis of this system is that it allows us to compare the predictions of the Voronoi tessellation with the actual data for the cavity. The calculated average volume of the cavity is 1.70 nm^3 , sensibly higher than the cavity volume which is 0.93 nm^3 . But the volume of the bubble, as computed with the Voronoi tessellation, also includes the volume occupied by the interfacial molecules which was not taken into account for the cavity's volume. Therefore we must subtract the interfacial volume, that consists of the number of interfacial molecules times the average volume per molecule multiplied by an unknown factor whose value is between from $1/2$ and 1 . This factor comes from considering two limiting cases. In the former case ($1/2$), the centers of the interfacial molecules are assumed to be located at the cavity boundary whereas in the latter one (1), the interfacial molecules are tangent to the cavity boundary. If we assume an intermediate factor ($3/4$) the volume of the

cavity calculated using the Voronoi tessellation is 0.98 nm^3 , very close to the actual volume of the artificial cavity.

B. Metastable and unstable water

In this section we analyze the Voronoi tessellation of water in conditions far from the thermodynamic stability. This is performed at two state points at 280 K, one above (-2250 bar) and the other below (-2630 bar) the liquid-vapor spinodal line corresponding to the metastable and unstable regions, respectively. In both cases the system cavitates spontaneously. Figure 6 represents the average volume of the system for two independent runs at $T=280 \text{ K}$, $p=-2250 \text{ bar}$. Notice that the density fluctuations before cavitation takes place are very similar in both runs and that the average volume is essentially constant along the simulations (before cavitation). The resulting average volume per molecule for this state is $\bar{V}=17.1 \text{ nm}^3$. Figure 6 also shows that cavitation happens stochastically: although the density fluctuations are akin in both runs, the cavitation times are sensibly different.

FIG. 6: Time evolution of the average volume per molecule for two runs of a point in the metastable region ($T=280 \text{ K}$, $p=-2250 \text{ bar}$). The sharp increase of the volume at the end of the simulations correspond to cavitation events.



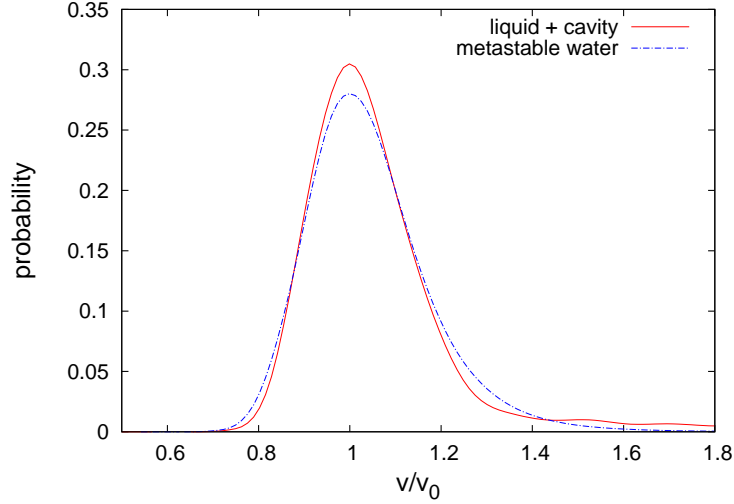
Our main goal is to study bubble nucleation from metastable and unstable liquid water using a local order parameter (the volume of the largest bubble) whose construction is based

on the Voronoi tessellation. Therefore, as previously shown, we need to define the proper parameters of the Voronoi Polyhedra. This problem differs from that commented in the previous section (detection of a cavity in a liquid) in several aspects. First, the created cavity was static, *i.e.*, the molecules in the liquid configurations had exactly the same positions as those in the system with the cavity. Thus, the VP properties of the molecules far away from the cavity were exactly the same in both systems. This allowed an unequivocal assignment of bulk and interfacial molecules and enabled us to safely investigate the features of the Voronoi Polyhedra for the latter particles. Bubbles forming in a metastable liquid are not static: they grow (and disappear) until, eventually, the system cavitates. A bubble may differ from an empty cavity because some reconstruction must take place at the interface, and also because of the presence of a small number of vapor molecules inside the bubble (the “cavity” is not empty now). However these vapor molecules should have, by definition, large VP volumes so the conditions imposed to tag a molecule as interfacial will also detect the vapor ones. Despite these differences, we may use the information obtained for the liquid with a cavity in order to interpret the results for metastable water.

A closer look at the differences between the properties of the Voronoi tessellations of liquid water with a cavity and metastable water is shown in Figure 7 where we present the distribution of VP volumes. Since the density is different, it seems important to scale the volumes using the average volume of the liquid molecules. In practice, we have applied a factor so that the maximum of the distributions appears at $V/V_0 = 1$. The curves for both systems show minor differences. Firstly, the distribution of volumes is wider for metastable water. Besides, there is a minor but significant difference in the large volumes region: the distribution in metastable water is smooth whereas the cavity gives rise to the appearance of wiggles. This seems to indicate that the abrupt inhomogeneity of the artificially created cavity is not present in the bubbles whose interface is somewhat blurred. Figure 7 illustrates that the analysis made in the previous section may also be acceptable for the detection of bubbles. We only need to scale the parameters in order to account for the differences in the average volume per molecule and the sharpness of the distribution.

In analogy to Fig. 5, Figure 8 shows the anisotropy of the Voronoi Polyhedra as a function of their volumes for 11 randomly selected configurations of metastable water. For comparison

FIG. 7: Distribution of the reduced VP volumes for metastable water ($T=280$ K, $p=-2250$ bar) compared to that of liquid water at ambient conditions with a cavity



we have also plotted the data for liquid water already shown in Fig. 5 but scaled so that the mapping of the distributions is maximized. In accordance, we have also scaled the line separating the interfacial molecules from the liquid molecules obtained for liquid water with a cavity. The line contains the point ($V=0.048$ nm³, $\alpha = 1.5$) and its slope is 18 nm⁻³. It can be seen that the region to the left of the straight line for metastable water is very similar to that for liquid water with scaled parameters. This indicates that an analogous criterion (now the straight line $\alpha = 1.5 - 18 * (V - 0.048)$ shown in Fig. 8) may be used in both systems to distinguish the liquid molecules from the interfacial (vapor) ones.

The corresponding plot for water at a pressure ($p=-2630$ bar) below the spinodal line (unstable water) is shown in Figure 9. We have also included the data for liquid water using the same scaling as in Figure 8. The bulk region is again quite similar in both systems but the number of interfacial molecules is much higher for unstable water. Besides, in this case, the high VP volume of some molecules (up to 0.4 nm³) seem to indicate that the latter are actually vapor molecules (not shown in the figure because, in order to compare with the previous ones, we use the same axes scales in all of the α - V plots).

FIG. 8: Anisotropic factor as a function of volume for metastable water (red crosses) compared to that of liquid water (empty blue circles). The black line $\alpha = 1.5 - 18 * (V - 0.048)$ separates liquid-like molecules from vapor (interfacial) molecules.

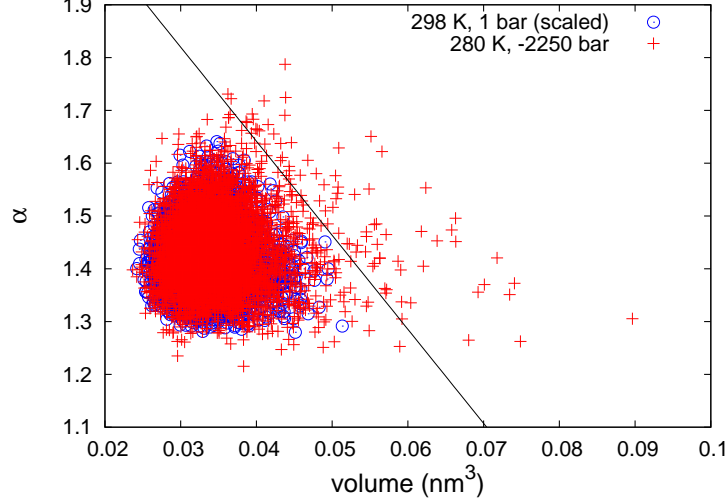
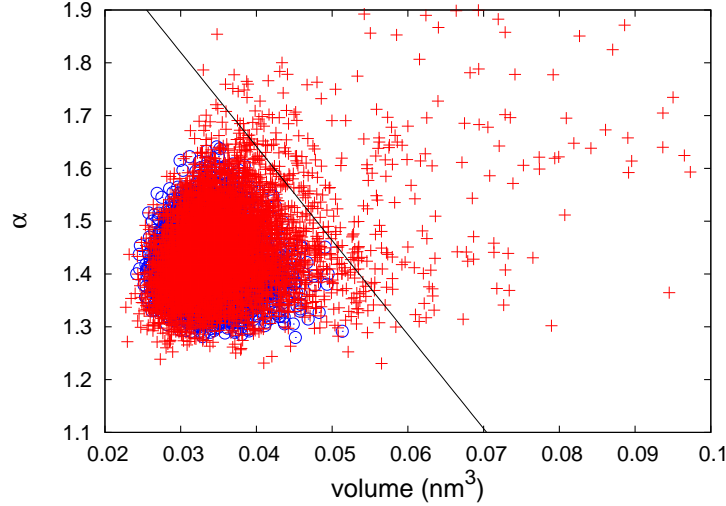


FIG. 9: Anisotropic factor as a function of volume for unstable water ($T=280$ K, $p=-2630$ bar) compared to that of liquid water with a cavity (scaled)



IV. MEAN FIRST-PASSAGE TIMES AND NUCLEATION RATES

Recently, Wedekind et al.²⁰ proposed a formalism —the mean first-passage time (MFPT) method— to investigate activated processes in those cases where they can be observed spontaneously in molecular simulations. In this work we have applied the method to investigate the nucleation rate of bubble formation in metastable water using the volume of the largest bub-

ble as the local order parameter. Bubbles are obtained by clustering together the molecules tagged as vapor (or interfacial following the criteria established in the previous section) that share a common face. Their volumes are the sum of the VP volumes of the particles belonging to a given cluster. Only the largest bubble, *i. e.*, the cluster with the largest volume, is required in the MFPT formalism. For each trajectory, we evaluate the time it takes to reach a given volume for the first time. Being nucleation a stochastic event, the cavitation time varies significantly from one run to another, as shown in Figure 10 for the system at $p=-2250$ bar. Moreover, Figure 10 also shows that at $p=-2250$ bar the time required to form a critical bubble is much larger than the time the system takes to cavitate. Once a bubble reaches a critical size it grows very quickly and destabilizes the system that cavitates. This indicates that nucleation and growth are not coupled. A comparison of this plot with Figure 6 shows that the volume fluctuations are independent of the size of the largest bubble except when the bubble size exceeds the critical one. In the latter case, the largest bubble grows very quickly and becomes a significant part of the total volume (notice that the divergences in both figures occur at the same time), and the system cavitates.

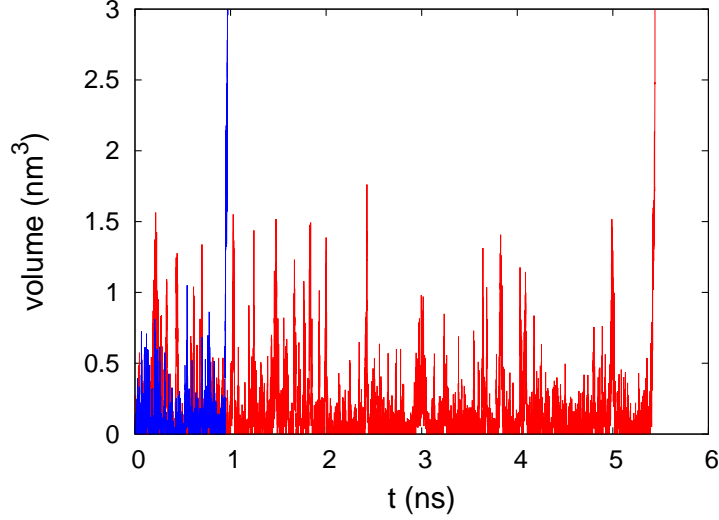
Fluctuations in Fig. 10 already enable us to have a rough idea of the size of the critical cluster (around 1.5 nm^3). However, for a precise estimate it is necessary to average the first passage times over a large number of trajectories for a given thermodynamic state. In this way we get a smooth MFPT curve from which it is possible to extract the rate and the size of the critical cluster. In particular, the MFPT reported in this work is the outcome of 200 independent simulation runs.

Figure 12 shows the comparison between the MFPT curve for metastable water (above the spinodal) with that of unstable water (below the spinodal). Notice that a different time scale is used for each of the curves. The nucleation behavior is quite different for these thermodynamic states. MFPT for metastable water shows a typical sigmoidal shape which can be fitted to a function of the form

$$\tau(V) = (\tau_J/2)\{1 + \text{erf}[c(V - V^*)]\}, \quad (3)$$

where $\text{erf}(x)$ is the error function. Wedekind *et al.*²⁰ have shown that the parameters of this equation provide relevant physical information. In particular, V^* is the size of the critical

FIG. 10: Time evolution of the volume of the largest bubble for the runs of Fig. 6



cluster (location of the transition state) and τ_J is the nucleation time which is related to the nucleation rate J by

$$J = \frac{1}{\tau_J V_s}, \quad (4)$$

where V_s is the system volume. Applying Eq. 3 to the system at $p = -2250$ bar, we obtain $\tau_J = 1.88$ ns, $V^* = 1.52$ nm³ and $c = 1.26$. From τ_J and V^* it is immediate to evaluate the nucleation rate and the radius of the critical cluster for which we obtain $J = 0.031$ ns⁻¹nm⁻³ and $r_{crit} = 0.71$ nm (assuming the critical cluster to be spherical). If we subtract the volume of the interfacial molecules, the volume of the critical cluster becomes 0.82 nm³, corresponding to a critical radius of 0.59 nm. A visual inspection of the critical and postcritical bubbles show that they are usually empty, i.e. no actual vapor molecules are within the bubble which is essentially made only of interfacial molecules. A snapshot of two bubbles, one slightly below the critical size and the other one larger than the critical bubble, are shown in Fig 11.

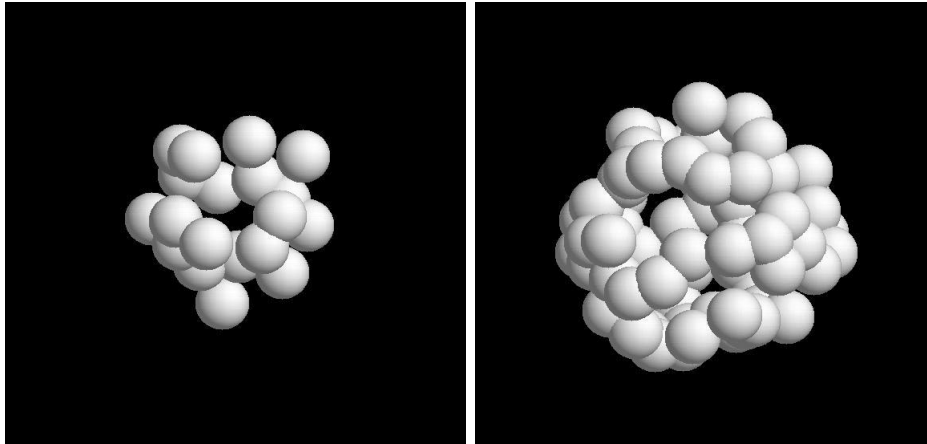
Our results may be compared to those coming from the Classical Nucleation Theory³ (CNT)

$$r_{crit}^{CNT} = \frac{2\gamma}{p_{sat} - p}, \quad (5)$$

$$J_{CNT} = \rho_N \left(\frac{2\gamma}{\pi m B} \right)^{1/2} e^{-\Delta G^{CNT}/kT}, \quad (6)$$

where γ is the interfacial tension, p_{sat} the coexistence pressure, m the mass of a molecule, ρ_N the number density of the liquid and B takes into account the mechanical equilibrium of

FIG. 11: A snapshot of the growth of a bubble. The image on the left corresponds to a precritical bubble and the image on the right corresponds to a postcritical one along the same trajectory (the configurations are separated by 0.02ps).

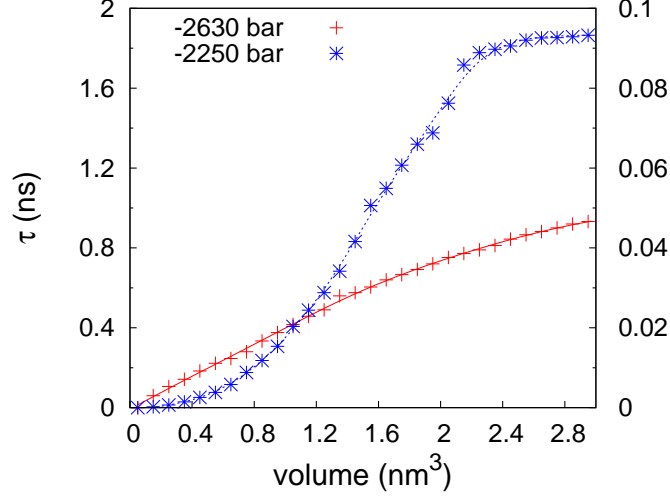


the bubble (in cavitation experiments $B=1$), and $\Delta G^{CNT} = W(r_{crit}^{CNT}) = (16\pi/3)(\gamma^3/(p_{sat} - p)^2)$. Assuming $\gamma \approx 73 \text{ mN/m}^{102}$, we obtain $r_{crit}^{CNT} \approx 0.67 \text{ nm}$, and $J_{CNT} = 1.7 \times 10^{-10} \text{ ns}^{-1}\text{nm}^{-3}$. Thus, the prediction of the CNT for the critical radius is quite accurate whereas the differences in the nucleation rates are about eight orders of magnitude. This is in agreement with the observations made for the Lennard-Jones system.¹⁴

On the contrary, the MFPT curve for unstable water is a monotonous function without an inflection point nor a plateau indicating that, in this case, nucleation and growth are coupled. A number of bubbles are quickly formed. When these bubbles grow, some of them eventually merge together giving rise to larger bubbles and the growth-coalescence process continues until cavitation (spinodal decomposition). This means that there is no nucleation free-energy barrier which is consistent with the fact that the system's pressure is below the spinodal.

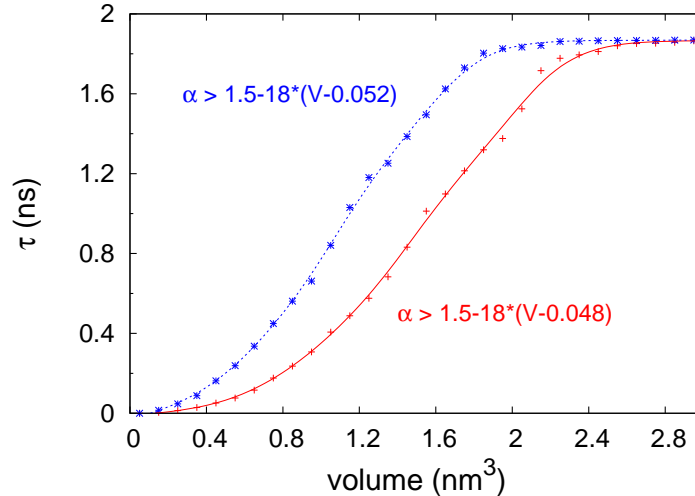
We now study how the choice of parameters affect the final results. Figure 13 shows the MFPT using two different criteria to distinguish liquid from vapor molecules. In both cases, we tag a molecule as vapor if its VP anisotropy, α , is above a straight line defined in terms of a pivotal point and a slope in the α -V plane. One of the curves correspond to the parameters provided by the study made in the previous section, $\alpha > 1.5 - 18 * (V - 0.048)$, and the other one has been obtained with $\alpha > 1.5 - 18 * (V - 0.052)$, a quite restrictive condition

FIG. 12: Comparison of the MFPT obtained for metastable and unstable TIP4P/2005 water at 280 K. Notice that a different scale is used for each of the curves (metastable liquid on the left axis and unstable on the right axis).



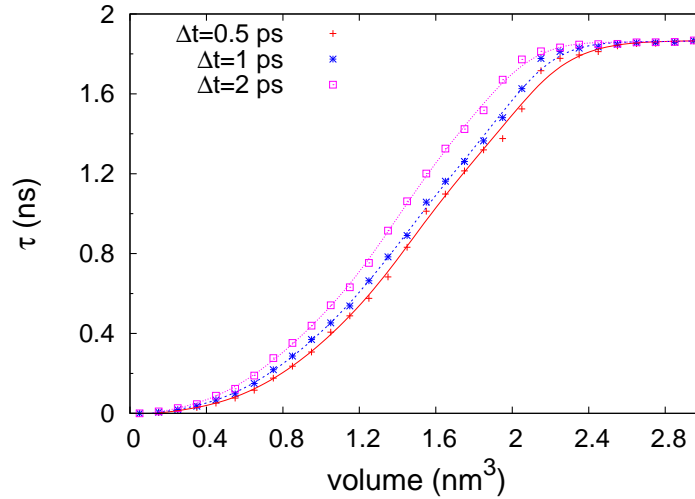
(see Fig. 8). A more restricted choice implies a smaller number of molecules fulfilling the condition and, as a result, the MFPT curve is shifted toward lower volumes. The size of the critical bubble is then slightly dependent on the choice of parameters. Interestingly, the value of τ_J (and, thus, the nucleation rate) does not depend at all on the definition of the order parameter. This is clear a demonstration of the robustness of the MFPT technique.

FIG. 13: MFPT for metastable water using two different VP parameters to distinguish liquid from “vapor” molecules.



Since the trajectories changes very little from one configuration to the next one, we only analyze them every Δt ps. Figure 14 shows the effect of modifying the sampling time Δt . Notice that sampling times sensibly larger than the simulation timestep can be used. In fact, an increase by a factor of four in Δt has a little effect on the size of the critical cluster and a null influence on the nucleation rate.

FIG. 14: MFPT for metastable water for two different sampling times (configurations are analyzed every Δt ps).



V. DISCUSSION AND CONCLUSIONS

In this work we set up a Voronoi-based tessellation procedure to determine the volume of the largest vapor bubble that allows us to study bubble nucleation in an over-stretched TIP4P/2005 metastable water. The parameters of the Voronoi polyhedra that allow to distinguish bulk (liquid) particles from interfacial (or vapor) ones have been obtained from the investigation of liquid configurations in which a cavity has been artificially created. It has been shown that best choice of parameters involves a combination of the Voronoi Polyhedra volume and nonsphericity factor α . The study allows to reduce to a minimum the intrinsic arbitrariness in fixing the parameters required to detect the growth of bubbles

in the metastable liquid. As a consequence the nucleation rate is completely independent on the parameters chosen to define the local order and the critical cluster size is only moderately dependent on them (the MFPT technique also contributes to this achievement).

One important open question is the effect of the finite-size. It has been pointed that the MFPT analysis is less sensitive to finite size effects than other approaches because it only requires a box large enough to contain several times the critical cluster.²⁴ Since our calculated volume of the critical cluster for metastable TIP4P/2005 water is 1.5 nm^3 and the average system volume is about 17 nm^3 , we conclude that our chosen system fulfils the required condition and we can neglect (at least, at this stage) finite-size effects.

As in simple fluids, the bubble nucleation rate estimated with Classical Nucleation Theory turns out to be much lower (8 orders of magnitude) than the one computed using MFPT. This could be due to the fact that CNT neglects curvature corrections to the surface free-energy of the bubble. When analyzing the mechanism of bubble formation above and below the spinodal, we observe clear differences. In the simulations of the liquid above the spinodal line, one bubble grows larger than all others in a fairly compact shape whereas, for the liquid below the spinodal line, we detect the formation of few bubbles which, eventually, merge to form larger ones (spinodal decomposition). However, above the spinodal we have also detected bubbles with different topologies, proving that small bubbles are strongly fluctuating objects. In the coming future, we plan to attempt a systematic characterization of the topology of the bubbles, as we believe it might play an important role in the cavitation process.

In general, the Voronoi tessellation is a relatively CPU-time consuming method. For a deeper investigation of the bubble nucleation mechanism it seems interesting to devise alternative ways of partitioning and calculating the bubble volume. Therefore, the results presented in this work can be seen as a benchmark for further bubble nucleation studies.

Acknowledgments

This work has been funded by grants FIS2010/16159 of the MEC, P2009/ESP-1691 of CAM and the Marie Curie Integration Grant PCIG-GA-2011-303941 (ANISOKINEQ) C.V. also acknowledges financial support from a Juan de La Cierva Fellowship. We acknowledge

Carlos Vega for helpful discussions and a critical reading of the manuscript.

- ¹ M. Shusser and D. Weihs, *Int. J. Multiphase Flow* **25**, 1561 (1999).
- ² K. S. Suslick, *SCIENCE* **247**, 1439 (1990).
- ³ M. Blander and J. L. Katz, *AICHE J.* **21**, 833 (1975).
- ⁴ Y. Viisanen and R. Strey, *J. Chem. Phys.* **101**, 7835 (1994).
- ⁵ P. E. Wagner and R. Strey, *J. Chem. Phys.* **80**, 5266 (1984).
- ⁶ M. M. Rudek, J. L. Katz, I. V. Vidsensky, V. Zdimal, and J. Smolik, *J. Chem. Phys.* **111**, 3623 (1999).
- ⁷ H. Lihavainen, Y. Viisanen, and M. Kulmala, *J. Chem. Phys.* **114**, 10031 (2001).
- ⁸ Y. J. Kim, B. E. Wyslouzil, G. Wilemski, J. Wolk, and R. Strey, *J. Phys. Chem. A* **108**, 4365 (2004).
- ⁹ M. Gharibeh, Y. Kim, U. Dieregswiler, B. E. Wyslouzil, D. Ghosh, and R. Strey, *J. Chem. Phys.* **122**, 094512 (2005).
- ¹⁰ E. Herbert, S. Balibar, and F. Caupin, *Phys. Rev. E* **74**, 041603 (2006).
- ¹¹ F. Caupin, *Phys. Rev. E* **71**, 051605 (2005).
- ¹² C. F. Delale, J. Hrubby, and F. Marsik, *J. Chem. Phys.* **118**, 792 (2003).
- ¹³ M. E. M. Azouzi, C. Ramboz, J.-F. Lenain, and F. Caupin, *Nature Physics* **advance online publication**, 1 (2012).
- ¹⁴ X. C. Zeng and D. W. Oxtoby, *J. Chem. Phys.* **94**, 4472 (1991).
- ¹⁵ V. Talanquer and D. Oxtoby, *Journal of Chemical Physics* **102**, 2156 (1995).
- ¹⁶ V. K. Shen and P. G. Debenedetti, *J. Chem. Phys.* **111**, 3581 (1999).
- ¹⁷ Z.-J. Wang, C. Valeriani, and D. Frenkel, *Journal of Physical Chemistry B* **113**, 3776 (2009).
- ¹⁸ S. L. Meadley and F. A. Escobedo, *J. Chem. Phys.* **137**, 074109 (2012).
- ¹⁹ M. A. Gonzalez, Master's thesis, Fac. Ciencias Quimicas, Univ. Complutense, Madrid (2011).
- ²⁰ J. Wedekind, R. Strey, and D. Reguera, *J. Chem. Phys.* **126**, 134103 (2007).
- ²¹ G. Chkonia, J. Woelk, R. Strey, J. Wedekind, and D. Reguera, *Journal of Chemical Physics* **130** (2009).
- ²² J. Wedekind, G. Chkonia, J. Woelk, R. Strey, and D. Reguera, *J. Chem. Phys.* **131**, 114506 (2009).

- ²³ J. Wedekind, J. Woelk, D. Reguera, and R. Strey, J. Chem. Phys. **127**, 154515 (2007).
- ²⁴ A. Perez and A. Rubio, J. Chem. Phys. **135**, 244505 (2011).
- ²⁵ B. Senger, P. Schaaf, D. S. Corti, R. Bowles, J. C. Voegel, and H. Reiss, J. Chem. Phys. **110**, 6421 (1999).
- ²⁶ J. Wedekind and D. Reguera, J. Chem. Phys. **127**, 154516 (2007).
- ²⁷ J. A. van Meel, L. Filion, C. Valeriani, and D. Frenkel, J. Chem. Phys. **136**, 234107 (2012).
- ²⁸ P. R. ten Wolde and D. Frenkel, J. Chem. Phys. **109**, 9901 (1998).
- ²⁹ A. Okabe, B. Boots, K. Sugihara, and S. N. Chiu, *Spatial Tessellations: Concepts and Applications of Voronoi Diagrams* (Wiley, New York, 2000).
- ³⁰ D. Eppstein, <http://www.ics.uci.edu/~eppstein/gina/voronoi.html>.
- ³¹ http://www.voronoi.com/wiki/index.php?title=Voronoi_Applications.
- ³² R. Karch, F. Neumann, M. Neumann, P. Szawłowski, and W. Schreiner, Ann. Biomed. Engin. **31**, 548 (2003).
- ³³ J. D. Bernal, Proc. R. Soc. London A **280**, 299 (1964).
- ³⁴ J. N. Cape, J. L. Finney, and L. V. Woodcock, J. Chem. Phys. **75**, 2366 (1981).
- ³⁵ J. C. Gil Montoro and J. L. F. Abascal, J. Phys. Chem. **97**, 4211 (1993).
- ³⁶ J. C. Gil Montoro, F. Bresme, and J. L. F. Abascal, J. Chem. Phys. **101**, 10892 (1994).
- ³⁷ R. Y. Yang, R. P. Zou, and A. B. Yu, Phys. Rev. E **65**, 041302 (2002).
- ³⁸ O. Gedeon and M. Liska, J. Non-Crystalline Solids **303**, 246 (2002).
- ³⁹ P. Jedlovsky, N. N. Medvedev, and M. Mezei, J. Phys. Chem. B **108**, 465 (2004).
- ⁴⁰ J. Q. Xu, R. P. Zou, and A. B. Yu, Granular Matt. **9**, 455 (2007).
- ⁴¹ M. Canales, Phys. Rev. E **79**, 051802 (2009).
- ⁴² O. Gedeon, M. Liska, and J. Machacek, J. Non-crystalline solids **357**, 1574 (2011).
- ⁴³ J. Skvor and I. Nezbeda, Mol. Phys. **109**, 133 (2011).
- ⁴⁴ A. Idrissi, I. Vyalov, M. Kiselev, M. V. Fedorov, and P. Jedlovsky, J. Phys. Chem. B **115**, 9646 (2011).
- ⁴⁵ M. Swart and P. T. Van Duijnen, Int. J. Quantum Chem. **111**, 1763 (2011).
- ⁴⁶ E. E. David and C. W. David, J. Chem. Phys. **76**, 4611 (1982).
- ⁴⁷ G. Neumayr, T. Rudas, and O. Steinhauser, J. Chem. Phys. **133**, 084108 (2010).
- ⁴⁸ V. P. Voloshin, N. N. Medvedev, M. N. Andrews, R. R. Burri, R. Winter, and A. Geiger, J. Phys. Chem. B **115**, 14217 (2011).

- ⁴⁹ M. Haberler, C. Schroeder, and O. Steinhauser, *Phys. Chem. Chem. Phys.* **13**, 6924 (2011).
- ⁵⁰ P. Jedlovszky, *J. Chem. Phys.* **113**, 9113 (2000).
- ⁵¹ P. Gomez-Alvarez, A. Dopazo-Paz, L. Romani, and D. Gonzalez-Salgado, *J. Chem. Phys.* **134**, 014512 (2011).
- ⁵² I. Hoedl, J. Hoedl, A. Worman, G. Singer, K. Besemer, and T. J. Battin, *PLOS ONE* **6**, e26368 (2011).
- ⁵³ F. B. Usabiaga and D. Duque, *Phys. Rev. E* **79**, 046709 (2009).
- ⁵⁴ B. Bouvier, R. Gruenberg, M. Nilges, and F. Cazals, *Proteins - Struct. Funct. Bioinformat.* **76**, 677 (2009).
- ⁵⁵ R. E. Isele-Holder, B. D. Rabideau, and A. E. Ismail, *J. Phys. Chem. A* **116**, 4657 (2012).
- ⁵⁶ A. Geiger, N. N. Medvedev, and Y. I. Naberukhin, *J. Struct. Chem.* **33**, 226 (1992).
- ⁵⁷ J. P. Shih, S. Y. Sheu, and C. Y. Mou, *J. Chem. Phys.* **100**, 2202 (1994).
- ⁵⁸ Y. I. Jhon, K. T. No, and M. S. Jhon, *Fluid Phase Equilibria* **244**, 160 (2006).
- ⁵⁹ G. G. Malenkov, *J. Struct. Chem.* **48**, 723 (2007).
- ⁶⁰ Y. L. Yeh and C. Y. Mou, *J. Phys. Chem. B* **103**, 3699 (1999).
- ⁶¹ P. Jedlovszky, L. B. Partay, A. P. Bartok, V. P. Voloshin, N. N. Medvedev, G. Garberoglio, and R. Vallauri, *J. Chem. Phys.* **128**, 244503 (2008).
- ⁶² G. Stirnemann and D. Laage, *J. Chem. Phys.* **137**, 031101 (2012).
- ⁶³ I. I. Vaisman, F. K. Brown, and A. Tropsha, *J. Phys. Chem.* **98**, 5559 (1994).
- ⁶⁴ P. Jedlovszky, *J. Chem. Phys.* **111**, 5975 (1999).
- ⁶⁵ M. Zapalowski and W. M. Bartczak, *Computers & Chem.* **24**, 459 (2000).
- ⁶⁶ M. Zapalowski and W. M. Bartczak, *Res. Chem. Intermed.* **27**, 855 (2001).
- ⁶⁷ A. Idrissi, P. Damay, K. Yukichi, and P. Jedlovszky, *J. Chem. Phys.* **129**, 164512 (2008).
- ⁶⁸ G. Neumayr, C. Schroeder, and O. Steinhauser, *J. Chem. Phys.* **131**, 174509 (2009).
- ⁶⁹ C. Schroeder, G. Neumayr, and O. Steinhauser, *J. Chem. Phys.* **130**, 194503 (2009).
- ⁷⁰ C. W. David, *Computers & Mathematics with Appl.* **12**, 763 (1986).
- ⁷¹ C. W. David, *Computers and Chemistry* **12**, 207 (1988).
- ⁷² R. A. Lewis, *J. Comp.-Aided Molec. Design* **3**, 133 (1989).
- ⁷³ M. G. Alinchenko, V. P. Voloshin, N. N. Medvedev, M. Mezei, L. Partay, and P. Jedlovszky, *J. Phys. Chem. B* **109**, 16490 (2005).
- ⁷⁴ D.-S. Kim, C.-H. Cho, D. Kim, and Y. Cho, *Computer-Aided Design* **38**, 431 (2006).

- ⁷⁵ M. Petrek, P. Kosinova, J. Koca, and M. Otyepka, *Structure* **15**, 1357 (2007).
- ⁷⁶ D. Kim, C.-H. Cho, Y. Cho, J. Ryu, J. Bhak, and D.-S. Kim, *J. Molec. Graph. & Model.* **26**, 1104 (2008).
- ⁷⁷ S. Sonavane and P. Chakrabarti, *PLOS Comput. Biol.* **4**, e1000188 (2008).
- ⁷⁸ D. Chakraborty and A. Chandra, *J. Molec. Liq.* **163**, 1 (2011).
- ⁷⁹ L. Wang and T. Ueda, *Ocean Engin.* **38**, 519 (2011).
- ⁸⁰ J. T. Fern, D. J. Keffer, and W. V. Steele, *J. Phys. Chem. B* **111**, 13278 (2007).
- ⁸¹ D. S. Kim, Y. Cho, and D. Kim, *Computer-Aided Design* **37**, 1412 (2005).
- ⁸² D. Kim and D.-S. Kim, *Computer-Aided Design* **38**, 417 (2006).
- ⁸³ W. Brostow, J. P. Dussault, and B. L. Fox, *J. Comput. Phys.* **29**, 81 (1978).
- ⁸⁴ J. L. Finney, *J. Comput. Phys.* **32**, 137 (1979).
- ⁸⁵ M. Tanemura, T. Ogawa, and N. Ogita, *J. Comput. Phys.* **51**, 191 (1983).
- ⁸⁶ N. N. Medvedev, *J. Comput. Phys.* **67**, 223 (1986).
- ⁸⁷ J. L. F. Abascal and J. C. G. Montoro, to be published.
- ⁸⁸ B. Hess, C. Kutzner, D. van der Spoel, and E. Lindahl, *J. Chem. Theory Comput.* **4**, 435 (2008).
- ⁸⁹ U. Essmann, L. Perera, M. L. Berkowitz, T. Darden, H. Lee, and L. G. Pedersen, *J. Chem. Phys.* **103**, 8577 (1995).
- ⁹⁰ J. P. Ryckaert, G. Ciccotti, and H. J. C. Berendsen, *J. Comput. Phys.* **23**, 327 (1977).
- ⁹¹ G. Bussi, D. Donadio, and M. Parrinello, *J. Chem. Phys.* **126**, 014101 (2007).
- ⁹² M. Parrinello and A. Rahman, *J. Appl. Phys.* **52**, 7182 (1981).
- ⁹³ J. L. F. Abascal and C. Vega, *J. Chem. Phys.* **123**, 234505 (2005).
- ⁹⁴ C. Vega, J. L. F. Abascal, M. M. Conde, and J. L. Aragones, *Faraday Discuss.* **141**, 251 (2009).
- ⁹⁵ C. Vega and J. L. F. Abascal, *Phys. Chem. Chem. Phys.* **13**, 19663 (2011).
- ⁹⁶ H. L. Pi, J. L. Aragones, C. Vega, E. G. Noya, J. L. F. Abascal, M. A. Gonzalez, and C. McBride, *Molecular Physics* **107**, 365 (2009).
- ⁹⁷ M. A. Gonzalez and J. L. F. Abascal, *J. Chem. Phys.* **132**, 096101 (2010).
- ⁹⁸ C. Vega, J. L. F. Abascal, and I. Nezbeda, *J. Chem. Phys.* **125**, 034503 (2006).
- ⁹⁹ Y. C. Liao, D. J. Lee, and P. J. He, *Powder Tech.* **123**, 1 (2002).
- ¹⁰⁰ O. Gedeon, *J. Non-Crystalline Solids* **351**, 1139 (2005).
- ¹⁰¹ A. Idrissi, I. Vyalov, P. Damay, M. Kiselev, Y. P. Puhovski, and P. Jedlovsky, *J. Molec. Liq.*

153, 20 (2010).

¹⁰² C. Vega and E. de Miguel, J. Chem. Phys. **126**, 154707 (2007).